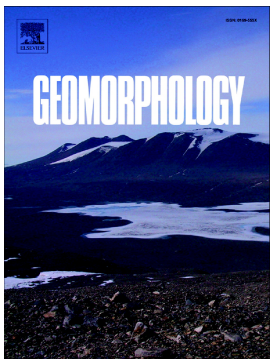

The effects of flood history on sediment transport in gravel-bed rivers

Luca Mao

PII: S0169-555X(18)30354-4
DOI: doi:10.1016/j.geomorph.2018.08.046
Reference: GEOMOR 6509

To appear in: *Geomorphology*

Received date: 20 March 2018
Revised date: 31 August 2018
Accepted date: 31 August 2018

Please cite this article as: Luca Mao , The effects of flood history on sediment transport in gravel-bed rivers. Geomor (2018), doi:10.1016/j.geomorph.2018.08.046

The effects of flood history on sediment transport in gravel-bed rivers

Luca Mao[1,2]

[1] Department of Ecosystems and Environment, Pontificia Universidad Católica de Chile, Santiago, Chile

[2] School of Geography, University of Lincoln, Lincoln, UK

Abstract

The transport of coarse sediment during floods often exhibits hysteresis patterns from changes in flow fields, channel geometry, bedforms, or sediment supply conditions. Flume experiments that simulate hydrographs tend to confirm that hysteresis is a consequence of the progressive organization of surface sediments in terms of grain protrusion, imbrication, orientation, and roughness. Hysteretic patterns are also highly dependent on the kind of sediment supply conditions, and the type of simulated hydrograph. A factor that has not been investigated extensively is the effect of the timing and sequencing of floods on bedload transport. Depending on its magnitude and duration, each flood leaves the channel bed in a different condition, which influences the bedload transport of the next event, representing the river bed's memory of past floods, which can determine future responses to natural disturbances. In this study, I investigated the effects of different sequences of events, i.e., the flood history, on sediment transport through a series of flume experiments that simulated three types of stepped and symmetrical hydrographs (ranging from short-duration/high-magnitude to long-duration/low-magnitude events) under sediment recirculation conditions. Hydrographs were simulated as a sequence of the same event, and with events in different sequences, in order to explore the effects of different antecedent

conditions on sediment transport. The results show that a previous event decreases the rates of sediment transported by a certain hydrograph by around 40% if a high-magnitude event precedes another one and around 70% if a low-magnitude event precedes another event of similar magnitude. A low-magnitude event does not affect the rate of sediment transported by a subsequent high-magnitude flood, but a high-magnitude event reduces the sediment transported by a subsequent long-duration/low-magnitude event.

Keywords: flume; hydrographs; hysteresis; flood history; gravel-bed rivers

1. Introduction

The evaluation and prediction of coarse sediment transport are essential for understanding fluvial system morphodynamics and play an important role in a wide range of river engineering and management interventions, such as stable channel design, sediment flushing, river restoration, and flood hazard planning (Church, 2006). However, field data are scarce because it is costly and difficult to measure bedload in the field (e.g., Vericat et al., 2006). Empirical formulas are available (e.g., Wilcock and Crowe, 2003), but these usually fail to accurately predict bedload transport (e.g., Barry et al., 2004; Vázquez-Tarrío and Menéndez-Duarte, 2015) because they generally derive from flume experiments that use steady flows (i.e., constant discharge over time) that do not approximate field conditions. Sediment transport occurs instead during floods, but few examples are available of continuous measurement of coarse sediment transport during high flows. The available evidence shows that bedload is highly nonlinear, and hysteretic effects are common. When the peak of sediment transport occurs before the peak of flow discharge, hysteresis is clockwise (e.g., Reid et al., 1985; Kuhnle, 1992), whereas it is counterclockwise when a

temporal lag exists between flow discharge and sediment transport peaks (e.g., Lee et al., 2004; Humphries et al., 2012).

Bedload transport hysteresis often occurs because of changes in the conditions of sediment availability during floods, which could be related to effects at the reach or basin scale. For instance, based on continuous records of coarse sediment transport in a glacierized Italian Alpine basin, Mao et al. (2014) showed that hysteresis is predominantly clockwise during the snowmelt period and counterclockwise during the glacier melting period, revealing changes in sediment availability over time at the basin scale. However, field data of bedload hysteresis are difficult to interpret because several processes that could be responsible for hysteretic patterns are at play at the same time (Gunsolus and Binns, 2018). Flume experiments that simulate hydrographs allow the invstigation of processes related to the role of sediment composition (sand vs. gravel), sediment supply conditions (fed vs. starved), and bed composition (armouring and surface sediment arrangements) on coarse sediment dynamics during floods. While relatively uncommon, flume experiments that simulate hydrographs have increasingly been reported in the literature in recent years (see Gunsolus and Binns, 2018).

Some flume experiments have shown clockwise hysteresis (bedload peak before the discharge peak), but this was mainly because of the lack of constant sediment supply (e.g., Hassan et al., 2006, Humphries et al., 2012). In other experiments, bedload hysteresis has been counterclockwise (Lee et al., 2004; Bombar et al., 2011), but this was explained by delays in passing sand dunes or late rupture of static armour. Based on a series of flume experiments of stepped hydrographs conducted under sediment recirculation conditions (i.e., creating a mobile armour layer), Mao (2012) showed that less sediment is transported during the falling than the rising limb of hydrographs (clockwise hysteresis). The grain size

of the bed remained virtually constant during hydrographs, thus corroborating the hypothesis that mobile armour persists throughout a flood (e.g., Wilcock and DeTemple, 2005), but the arrangement and composition of surface sediment changes after the simulated hydrographs (Mao, 2012). The presence of an armour layer affects sediment transport and hysteresis. For instance, Guney et al. (2013) showed that hysteresis during a simulated hydrograph is clockwise if the bed is not armoured and counterclockwise if the bed is armoured before the simulated hydrograph.

Little flume evidence available about the role of individual floods on sediment transport (Karimaee Tabarestani and Zarrati, 2015; Gunsolus and Binns, 2018) and even less knowledge about the effects of flood history on bedload transport in gravel-bed rivers. Flood history is considered here as the sequence of floods of different magnitudes and duration to which a channel bed has been exposed prior to a particular event. Even flows below the threshold for incipient grain motion can also change the critical shear stress required to move sediments (Haynes and Pender, 2007) because of the development of coarse grain clusters (Piedra et al., 2012) or vertical winnowing of finer sediments (Curran and Waters; 2014; Powell et al., 2016).

Based on field observations, Reid et al. (1985) indicated that sediment entrainment during isolated floods requires higher shear stress than what is needed for floods that follow one closely after another. Frostick et al. (1984) suggested that past floods control the proportion of fine sediment infiltrated into the coarser matrix, changing the sediment transport conditions of future floods. Marquis and Roy (2012) made similar observations, reporting that bed dilation/contraction (caused by fine sediment infiltration or winnowing in a gravel framework) relate to bed conditions left by previous events, highlighting the role of flood history on sediment transport in gravel-bed rivers. However, the role of antecedent flows

and floods on sediment transport in rivers is far from having been adequately explored. Water and Curran (2015) conducted one of the few flume experiments with repeated hydrographs. They confirmed Mao's (2012) findings on sediment transport hysteresis owing to surface structure adjustments, adding the stabilizing effect of low previous flows, and developing a useful parameter to improve bedload predictions depending on the hydrograph limbs for which calculations are needed. However, because sequences of floods of different magnitudes and duration have never been simulated, only scattered evidence are currently available. Thus, knowledge of the processes involved in gravel entrainment and transport in naturally variable regimes is still incomplete.

This paper reports on a series of flume experiments that simulated three stepped hydrographs of different magnitudes and duration in different sequences, under sediment recirculation conditions. The sequences were designed to simulate three repetitions of the same hydrograph and also hydrographs in different sequences, such as hydrographs of increasing magnitude, decreasing magnitude, a sequence with a low-magnitude event between two high-magnitude events, and a sequence with the reverse arrangement. The aim is to explore the role of previous floods, or flood memory, on bedload transport. The experiments were designed to test the hypothesis that, under sediment recirculation conditions, previous events reduce sediment transport of subsequent floods of the same magnitude and duration,and that high-magnitude events are more effective than low-magnitude events in reducing sediment transport of subsequent events.

2. Materials and methods

Experiments were conducted in an 8-m-long, 0.3-m-wide tilting flume. The setup and operational protocol of the experiments were the same as those described in Mao (2012). The flume with sediments was 6 m long, and part of the upstream and downstream sections had an artificially roughened bed in order to adjust the flow. The sediment mixture was 20% sand and 80% gravel, with D_{16} = 1.7 mm, D_{50} = 6.2 mm, and D_{84} = 9.8 mm. Sediment was collected in a trap at the downstream end of the flume, weighed, and then recirculated by manually carrying the trap to the upstream end of the flume and returning the sediments to the fixed roughened bed. All of the sediment captured in the bedload traps was manually recirculated at intervals ranging from 1 to 10 min depending on the bedload transport rate; at least 200 g of sediment was collected prior to emptying the traps. The capture efficiency of the bedload traps was > 95%, even at the highest transport rate. During the experiments, the bed surface remained flat, with the appearance of small migrating sand sheets of negligible height only during the highest discharge runs (Mao, 2012).

A constant slope of 0.01 m m^{-1} was employed in all the experimental runs, with unit discharges ranging from 0.024 to 0.085 m^2 s^{-1}.

The discharges used to generate the hydrographs were selected to match the discharges used in a previous set of experiments (Mao et al., 2011), where all runs involved steady flows with sediment recirculation (Table 1). The experiments started by running a steady discharge of 0.031 m^2 s^{-1} for four hours to establish a water-worked surface with partially mobile grains (Mao, 2012). The discharge was then increased in steps to generate hydrographs. The runs simulated stepped hydrographs, with three rising steps, one flow step at the peak, and three symmetrical falling steps. As reported in Mao (2012), three different hydrographs were simulated: H representing a short-duration / high-magnitude event (105 min long, peaking at 0.085 m^2 s^{-1}), L representing a long-duration / low-

magnitude event (840 min long, peaking at 0.044 m^2 s^{-1}), and M representing an intermediate-duration moderate event (420 min long, peaking at 0.054 m^2 s^{-1}). In this paper, I present the results of experiments simulating these three hydrographs in different sequences (Table 1). Specifically, I simulated three sequences that consisted of three hydrographs each with the same duration and magnitude (HHH, MMM, and LLL), a hydrograph sequence of increasing magnitude and another of decreasing magnitude (i.e., LMH and HML respectively), a sequence with a low-magnitude event between two high-magnitude events (HLH), and a sequence with the reverse (LHL).

As stated in Mao (2012), the hydrographs were not intended to represent a specific field prototype, but rather a moderately sloped and narrow (~ 10 m wide) gravel-bed river (applying an undistorted 1/30 Froude scaling), as the main objective was to explore processes and interactions between sediment transport and surface grain size dynamics under sediment recirculating conditions and to simulate hydrographs.

During the simulated hydrographs, the flow was stopped at the end of each step and the flume drained in order to photograph the surface sediment in a 1.5 x 0.15 m area along the lower part of the flume. The photos were taken with a 12 MP digital camera. The grain size of surface sediments was obtained using a point-count technique, by digitizing the *b* axes of at least 600 particles located at the intersection of a grid superimposed on the photograph (i.e., point spacing of ~ 20 mm; see Mao, 2012, for further details).

3. Results and analysis

3.1. Repetitions of the same hydrographs

Three runs simulated three repetitions of the same hydrograph. The repetitions of the H series resulted in the highest sediment transport rates, which ranged from 118.47 to 1.01 g m^{-1} s^{-1}. Figure 1 shows that sediment transport rates were higher during the rising than the falling limb of the H hydrographs. For instance, for the first H event, with an intermediate discharge of 0.054 m^2 s^{-1}, the transport rates were 33.68 and 24.92 g m^{-1} s^{-1} during the rising and falling limbs respectively. As expected, the grain size of transported material varied, being coarser with the largest discharges. The D_{84} of transported material peaked at 10.19 mm (which exceeded the D_{84} of the mixture) during the peak discharge of the first H event. Interestingly, the grain size of the transported material increased in the subsequent hydrographs The D_{84} was 10.3 and 10.53 mm in the second and third H hydrographs respectively.

Higher sediment transport rates during the rising rather than the falling limbs could be appreciated visually for the MMM runs as for the HHH (Fig. 1). For the sequence of intermediate M events, the reduction in sediment transport from one event to the next was even more evident. For instance, at the maximum discharge of 0.054 m^2 s^{-1}, the transport rate peaked at 23.04, 18.73, and 5.54 g m^{-1} s^{-1} in the first, second, and third M events respectively. The grain size of transported sediments varied with discharge, but in this case, D_{50} and D_{84} did not increase from one event to the next as they did in the HHH series.

The transport rates in the repetitions of the long-duration low-magnitude events (LLL) ranged from 6.52 to 0.001 g m^{-1} s^{-1} (Fig. 1). The higher level of sediment transport during the rising limb was clearly evident with the first L event (0.54 and 0.035 g m^{-1} s^{-1} at 0.031 m^2 s^{-1} in the rising and falling limbs respectively) but was less evident in the second and third hydrographs. However, there was a marked reduction in sediment transport at the peak from the first to the third L event, going from 6.52 to 2.12 g m^{-1} s^{-1}.

Figure 2 shows the relationships between liquid discharge, transport rates, and surface and transported grain sizes (D_{50} and D_{84}) in all the sequences with repetition of the same hydrographs. As expected, transport rates increased in all cases with increased levels of liquid discharge. Transport rates were higher during the rising limbs than in the falling limbs for most hydrographs. Figure 2 shows the sediment transport rate at near-equilibrium conditions obtained during long-duration steady runs using the same discharges as used in building up the hydrographs (see Mao et al., 2011, for further details about these experimental runs). Figure 2 shows that sediment transport rates were generally higher than at equilibrium conditions for all flow steps of the HHH sequence. This was expected, as in all flume experiments with sediment recirculation, the transport rate reached the highest intensity at the beginning of the run and then progressively decreased as mobile armour developed and surface sediment became more structured (Marion and Fraccarollo, 1997; Mao et al., 2011).

The flow steps in the H hydrograph experiments were short (15 min), which was not enough time for the bed to develop a structured mobile armour. Interestingly, transport rates approached the values at near-equilibrium conditions for the third H hydrograph because the channel bed had experienced sufficient coarse sediment transport to develop a mobile armour layer. In contrast to static armour, which typically develops with selective transport of finer sediments under zero-feeding conditions (Church et al., 1998), the coarser mobile armour is created by kinematic sorting (Wilcock, 2001) in which all available grain sizes are transported, including the coarsest (Parker et al., 1982; Parker and Toro Escobar, 2002). Even the sediment transport rates in the first of the LLL runs approached the values at near-equilibrium conditions, probably because the low flow strength transported only small- to medium-sized grains and because the flow steps are considerably longer (120

min), which is enough time for the surface grains to become organized in terms of roughness, imbrication, clustering, and grain orientation, as Haynes and Pender (2007), Humphries et al. (2012), Piedra et al. (2012), and others have shown.

Figure 2 shows that the grain size of transported sediment increased with rise in the level of discharge and that the sediment transported in the falling limbs was always finer than that transported in the rising limbs. The coarsening of sediment transport in the falling limb (whether H, M, or L) is in agreement with the lower transport rates after peak flow. Mao (2012) had already pointed this out, but here this tendency is repeated in the second and third hydrographs of all the sequences. Figure 2 also shows that the grain size of surface sediment did not change significantly during the hydrographs. As Mao (2012) stated, this confirms the persistence of a mobile armoured layer in a fluvial system with unlimited sediment supply of all sizes, as observed in certain fields (Clayton and Pitlick, 2008) and experimental conditions (Wilcock and DeTemple, 2005). This paper adds to this evidence with the observation that this is true after repetitions of hydrographs, irrespective of their magnitudes and duration. Although the surface grain size does not change substantially during an event, the size of sediments increases with repetitions, which is probably caused by vertical winnowing of finer sediments over the coarser framework. The coarsening of the mobile armour layer produced by vertical winnowing is more evident for the HHH than the LLL sequence, which supports the theory of vertical kinetic winnowing of finer sediment (as in Bacchi et al., 2014), given that this process is likely to occur when coarser sediment has been moved and the layer of active sediment is thicker.

3.2. Simulation of hydrographs in different sequences

Simulations of hydrographs in different sequences produced similar results to the experiments simulating the same hydrographs in sequences, in terms of sediment transport rates, transported sizes, and surface grain sizes (Fig. 3 and Fig. 4). Sediment transport rates were higher and grain size was coarser in the rising limbs of the hydrographs, while surface grain size was unaffected by the magnitude of the simulated hydrograph (Fig. 3). Figure 3 allows a comparison of similar hydrographs simulated in different sequences. For example, hydrograph L in the LMH sequence transported significantly more sediment than did the corresponding L event in the HML sequence. Indeed, at their peak discharge (0.044 m^2 s^{-1}), the two hydrographs transported 3.91 and 0.31 g m^{-1} s^{-1} respectively, whereas at the lower discharge at the end of the events (i.e., step 7), they transported 0.004 and 0.000009 g m^{-1} s^{-1} respectively. Thus, a low-magnitude event transports considerably less sediment if proceeded by higher magnitude events. On the other hand, hydrograph H in the HML sequence transported at its peak nearly the same rate of sediment as did the corresponding H event in the LMH sequence. Indeed, at their peak discharge (0.085 m^2 s^{-1}), the two hydrographs transported 98.59 and 92.12 g m^{-1} s^{-1} respectively. Thus, a low-magnitude event transports considerably less sediment at its peak if it was proceeded by higher magnitude events; whereas a high-magnitude event was not affected by the occurrence of lower magnitude events before, and the transport rate at its peak did not depend on antecedent flow conditions.

3.3. Sediment transport at the peak of the hydrographs

I compared average sediment transport rates of all the flow steps to precisely quantify the role of antecedent events in reducing transport rates. For the sake of clarity, Fig. 5 shows only the average sediment transport rates at the peak of each hydrograph for all simulated

sequences. Transport rates of the second and third repetitions of sequences with repetitions of the same event (i.e., HHH, MMM, and LLL) clearly decreased, irrespective of the type of hydrograph. When sequences of different hydrographs were simulated, the reduction in sediment transport was strongly affected by the magnitude of the previous event. The transport rates at the peaks of the H events in the LMH and the HML sequences are around the same (98.59 and 92.12 g m^{-1} s^{-1} respectively). In other words, the H event transported the same amount of sediment when it is the first event of the sequence or the third event after two lower magnitude events (L and M events in this case). Interestingly, the M event transported slightly less if preceded by a H rather than a L hydrograph (9.58 *vs.* 14. 31 g m^{-1} s^{-1} respectively; Fig. 5). Considering the transport at the peak of the L event in LMH and HML, if the L event was preceded by a higher-magnitude event, the sediment transported at the peak was one order of magnitude less (3.91 *vs.* 0.32 g m^{-1} s^{-1}).

The results of the HLH and LHL sequences were similar (Fig. 5). For example, evidence show only a little difference between the transport rates of the first H event at peak in the HLH sequence and the H event in the LHL sequence, where it follows a lower-magnitude event L (97.51 *vs.* 131.23 g m^{-1} s^{-1}). The transport rate of the L event is one order of magnitude lower if it is preceded by a L or H event than if it is the first event of the sequence (0.76 *vs.* 5.69 g m^{-1} s^{-1}). The transport rate of the L event is remarkably similar if preceded by a H event, or by a L and H event (0.80 *vs.* 0.76 g m^{-1} s^{-1}), which shows that the effect of the H event is dominant over the effects on the channel bed of a long-duration but low-magnitude L event.

3.4. Hysteresis of sediment transport and transported grain size

Several flume studies have verified the existence of hysteretic patterns in the rate of sediment transported at the rising and falling limbs of hydrographs. In a recent review, Gunsolus and Binns (2018) showed that gravel-bed streams under sediment feeding conditions most commonly feature clockwise hysteresis (i.e., higher sediment transport during the rising limb). The authors suggested that the shape, duration, and magnitude of the hydrograph, along with sediment supply conditions, determine the hysteresis patterns and the processes responsible for such behavior. If morphological factors (e.g., planform and cross-sectional geometry, bedform migration) and factors related to limited or zero sediment feeding (e.g., static armour breakup) are excluded as causes of hysteresis, hysteresis must be caused by changes in the grain size of transported sediments or by changes in the grain size or spatial organization of surface clasts (as shown in Mao, 2012). These rather simplified conditions are verified in the experimental setting used in the present study, as no bedforms were allowed because of the flume setup and because sediments were continuously recirculated. The sequence of events here also allowed the investigation of the changes in hysteresis from one event to the next. Indeed, hysteresis can be considered as dependent not only on the values of driving variables (e.g., sediment supply, grain size, flow strength) but also on the values of the past driving variables. The idea that antecedent precipitation strongly affects the hydrological response of a hillside or catchment is well established in hydrology (e.g., Haynes, 1930; Norbiato and Borga, 2008; Camporese et al., 2014). In this study, hysteresis helps in quantifying the effects of flood history on sediment transport. Several ways to numerically quantify the direction and magnitude of hysteretic patterns are available in the literature (see Zuecco et al., 2016). In this study, I used the hysteresis index of Langlois et al. (2005), which was developed to analyze the temporal dynamics of liquid discharge and suspended sediment transport (e.g.,

Mao and Carrillo, 2017). The Langlois index is calculated as the ratio of the area below the regression lines fitted with the rising and falling limb hydrograph data. It is well suited for the present data set because the hydrographs are always specular and symmetrical, thus the discharges in the two limbs coincide and the areas are calculated using the same minimum and maximum discharges. Since the hysteresis index (H) is calculated as a ratio, a value of 1 means a lack of hysteresis, $H > 1$ indicates clockwise hysteresis, and $H < 1$ indicates counterclockwise hysteresis.

Figure 6 shows that the first hydrograph of the simulated sequences is always clockwise (as already pointed out by Mao, 2012). The H index ranges from 1.03 to 1.49 (average value 1.23). More interestingly, the hysteresis progressively reduces over time. There is either no hysteresis or counterclockwise pattern by the third event of all the series, as the H index ranges from 1.05 to 0.85 (average value 0.95). The clockwise bedload pattern in the first event of the series is related to a counterclockwise pattern of transported grain size (H ranges from 0.98 to 0.89, with an average value of 0.95; Fig. 7). In other words, the rising limb transports more but finer sediments than the falling limb, when the sediment transport rate is lower but sediments are coarser. This is in agreement with what Mao (2012) and Wang et al. (2015) observed for bimodal sediment mixtures. This process, along with the complex dynamics of progressive sediment organization and the development of coherent structures at the scale of clusters and patches (Waters and Curran, 2015; Powell et al., 2016) help to explain the changes in sediment transport patterns over multiple time scales and can improve predictions for individual floods.

4. Discussion

4.1. Antecedent floods and sediment transport

This study presents some of the first evidence on the effects of antecedent floods on sediment transport. Figure 8 summarizes the main findings from the seven simulated sequences. The role of antecedent events on sediment transport was calculated as percentage differences in average transport rates between given hydrographs and preceding ones. The percentage differences were calculated for the values of average transport rates for each of the seven flow steps that composed the simulated hydrographs. The results were grouped and discussed into five main categories of antecedent flow conditions (Fig. 8):

- **H after H**: In three cases a short-duration / high-magnitude flood was simulated following a similar event, namely the second event in the HHH sequence after the first (H2-H1 in HHH) and the third event after the second (H3-H2 in HHH), and the third H event after the first H event in the HLH sequence (H3-H1 in HLH). In the three cases, the transport rate of the second H event was around 40% lower than that of the previous one. A L event between two H hydrographs did not cause any further reduction in the transport rate of the second H event. In other words, a low-magnitude event does not play a major role in determining the sediment transported by a subsequent high-magnitude flood. The reduction in sediment transport from the first to the second event is probably caused by coarser sediments being mobilized from a thicker layer of active sediments (Curran and Waters, 2014). A further reason for this reducion is the fact that finer sediments infiltrate further into the moving gravel framework (Dudill et al., 2017) in a process known as kinetic sieving (Ferdowsi et al., 2017), which reduces the quantity of finer sediments available for a subsequent event. However, because of the short duration of the event, a mobile bed that is structured in terms of grain orientation, imbrication, and sediment clustering cannot be formed (Haynes and Pender, 2007;

Humphries et al., 2012; Mao, 2012), and the reduction in sediment transport does not exceed 40%.

- **M after M**: When a M event follows another one (M2-M1 and M3-M2 in the MMM sequence), sediment transport in the second event decreases by 40 to 70%, which represent a greater degree of variation than in the H events.
- **L after L**: In three cases a L event followed another one, namely the second event in the LLL sequence (L2-L1), the third after the second event in the LLL sequence (L3-L2), and the third L event after the first in the LHL sequence (L3-L1 in LHL). Sediment transport in the second event decreased by 45 to 85% (average around 70%), which is a wider range than that between two L events. Thus, a L event reduces the sediment transport of a following L event by more than what a H event affects a following H event. This is probably because the low-magnitude but long-duration flow steps allow surface sediments to adjust and organize clusters and patch structures. This change the standard deviation of the surface topography (Haynes and Pender, 2007; Ockelford and Haynes, 2013) and the protrusion of the coarsest grains (Masteller and Finnegan, 2017), which reduces the availability of sediments to be transported by the second L event.
- **H after L**: The direct effects of a L event on a following H event are evident if we compare the H event of the LHL or LMH sequence to the H event of a sequence in which H is the first hydrograph (HHH in this exercise). Figure 8 shows that the reduction in sediment transport in the second event is negligible (ranging from +10 to -20%), indicating that the sediment transported by a high-magnitude event is marginally affected by a previous long-duration / low-magnitude flood. Arguably, the surface structures created by a low-magnitude event that is only able to entrain medium-sized

grains can easily be destroyed by a higher magnitude flood in which even the coarsest sediments can be removed.

- **H after L**: The direct effects of H event on a following L is evident by comparing the L event of the HLH or HML sequence to the L event of the LLL sequence. In this case, the reduction of sediment transport in the second event is very high (up to 90%), demonstrating that a previous high-magnitude event can strongly affect the transport of a subsequent low-magnitude flood. The reduction of sediment transport is likely to be related to the reduction of finer sediment to be transported because of fine sediment infiltration into the coarser mobile armour layer (Dudill et al., 2017).

4.2. Implications

Sediment transport is a complex process that depends on a series of variables acting at either the basin (sediment availability, sediment connectivity, etc.), reach (geometrical channel changes, dynamic of bedforms, etc.), or local scale (dynamic of the armoured layer and sediment clusters, fine sediment infiltration, etc.). In addition to the time scale at which sediment transport shapes the bed (Recking et al., 2012; Rickenmann, 2018), the precise sequence of floods of different magnitudes determines the dynamics and rates of sediment transport. This study shows that antecedent conditions, and especially the sequencing of events, are indeed important factors to be considered in predicting sediment transport during floods, as sediment transport could be reduced by 70 to 40% if a hydrograph is preceded by a similar one, in the case of high- and low-magnitude events respectively. Interestingly, high-magnitude events determine sediment transport of the following lower-magnitude hydrographs.

Sequencing is thus of crucial importance for understanding the response of fluvial gravel-bed systems to climate change and changes in land and water use at the basin scale to reveal the effects of flood sequences of different magnitudes and duration on sediment transport. The expected climate change induced impacts on fluvial systems are likely to result in increased magnitude and frequency of higher floods with longer drought periods, along with a potential shift in timing of seasonal hydrological regimes (Baynes et al., 2018) that in Mediterranean climates with snowfall in winter can result in a even increased severity and frequency of extreme events (e.g., Bozkurt et al., 2017). Under these likely scenarios of changing flooding patterns (e.g., Salathe et al., 2014; Mallakpour and Villarini, 2015) it seems important to consider the sequence of floods events in order to assess river stability, river enhancement and restoration projects. Practical applications from the hydraulic and geomorphological points of view could range from changing the operation to hydropower plants in order to reduce the magnitude of higher floods, to managing connectivity at the basin scales for supplying sediments when needed in the hydrographic network. Also, as pointed out by Mao (2012), the recent availability of a low-cost detailed description of grain size, cluster organization, and even porosity of river surface (see Woodget et al., 2018; Seitz et al., 2018) could help to decipher the signature left by previous events and to infer conditions of sediment transport dynamics of following floods. As pointed out by Baynes et al. (2018), sequences of floods which consider a shift in the magnitude or frequency of forcing are rarely considered in physical models, and more experiments of this kind would be needed in future. Future attempts of expanding the extent of the present study, could try to simulate hydrographs of different shapes (i.e., asymmetrical hydrographs such as in Hassan et al., 2006) and also to simulate different durations of under threshold flows between hydrographs, which is likely to considerably

reduce sediment transport of subsequent low-magnitude events (see Haynes and Pender, 2007). Furthermore, it is worth pointing out that the runoff volume of the three types of hydrographs was different in the present study, and this does not allow me to compare the volume of sediment transported by different events. In this sense, further experiments simulating hydrographs of similar volumes could facilitate this comparison. As vertical sediment winnowing seems the main process driving the reduction of sediment transport of subsequent hydrographs of the same type, future experiments simulating sequences of hydrographs should quantify precisely the amount and temporality of fine sediment infiltration on the coarser gravel matrix (see, e.g., Dudill et al., 2017). Finally, the results presented in this study are intrinsically related to the nature of sediment feeding during the flume experiments. By recirculating sediments, the surface grain size tends to be invariant and independent of sediment transport rate and size (Wilcock and DeTemple, 2005), and the hysteresis during the hydrographs and reduction of sediment transport over time is mainly attributable to infiltration of fine sediments and progressive organization of grains and sediment clusters in the bed surface. Sediment recirculation is the condition that one could arguably consider representative of a natural river during a single flood (Wilcock and DeTemple, 2005). However, over longer time periods changes of sediment supply, development of bedforms, and morphological adjustments of cross sections could happen, thus invalidating the assumption that sediment recirculation is the best way of representing sediment input in a river system. Further studies simulating a variable input of sediment rates and sizes could prove useful in this sense.

5. Conclusions

A series of flume experiments were conducted in order to verify the effects of antecedent events on sediment transport in stepped hydrographs under sediment recirculation conditions. The results show that the hydrographs transport more but finer sediment during the rising limbs (clockwise hysteresis for bedload rates, and counterclockwise for grain size). Hysteresis decreases after the first event, probably because of the progressive vertical winnowing of finer sediments below the mobile armour layer, although the grain size of the surface sediments does not change substantially during events and after three repetitions. Under sediment recirculation conditions, a previous event diminishes the sediment transport rate of a given hydrograph. The evidence shows that sediment transport decreases by around 40% if a high-magnitude event precedes a similar one, probably becaue of vertical winnowing of finer sediment fractions. The reduction is more pronounced (around 70%) if a low-magnitude event precedes a similar one, and in this case the reason is related mainly to the progressive structuring of the mobile armour layer in terms of sediment orientation, imbrication, and clustering. A low-magnitude event does not play a major role in determining the rates of sediment transported by a subsequent high-magnitude flood. However, if a high-magnitude event precedes a long-duration / low-magnitude one, the effects on sediment transport are significant.

Acknowledgements

This research was supported by Fondecyt Regular Project 1170657 and Marie-Curie IEF Project 219294. Lynne Frostick and James Cooper provided many useful suggestions regarding the flume experiments. Diego Ravazzolo helped in digitizing grains on the photos, and Ricardo Carrillo helped with the analysis of the hysteresis index. The author

also thanks two anonymous reviewers, the Editor, and the Associate Editor for their careful reading and useful comments on the paper

References

Bacchi, V., Recking, A., Eckert, N., Frey, P., Piton, G., Naaim, M., 2014. The effects of kinetic sorting on sediment mobility on steep slopes, Earth Surf. Proc. Land., 39, 1075-1086. doi:10.1002/esp.3564.

Barry, J.J., Buffington, J.M., King, J.G., 2004. A general power equation for predicting bedload transport rates in gravel bed rivers. Water Resour. Res. 40, W104001. http://dx.doi.org/10.1029/2004WR003190.

Baynes, E.R.C., van de Lageweg, W.I., McLelland, S.J., Parsons, D.R., Aberle, J., Dijkstra, J., Henry, P., Rice, S.P., Thom, M., Moulin F., 2018. Beyond equilibrium: Re-evaluating physical modelling of fluvial systems to represent climate changes. Earth-Science Reviews 181, 82-97. https://doi.org/10.1016/j.earscirev.2018.04.007.

Bombar, G., Elci, S., Tayfur, G., Guney, M.S., Bor, A., 2011. Experimental and numerical investigation of bed-load transport under unsteady flows. J. Hydraul. Eng. 137(10), 1276–1282. doi:10.1061/(ASCE)HY.1943–7900.0000412.

Bozkurt, D., Rojas, M., Boisier, J.P., Valdivieso, J., 2017 Climate change impacts on hydroclimatic regimes and extremes over Andean basins in central Chile. Hydrol. Earth Syst. Sci. Discuss. https://doi.org/10.5194/hess-2016-690.

Camporese, M., Penna, D., Borga, M., Paniconi, C., 2014. A field and modeling study of nonlinear storage–discharge dynamics for an Alpine headwater catchment. Water Resour. Res. 50, 806-822.

Church, M., 2006. Bed material transport and the morphology of alluvial river channels. Annu. Rev. Earth Planet. Sci. 34(1), 325-354.

Church, M., Hassan, M.A., Wolcott, J.F., 1998. Stabilizing self organized structures in gravel-bed stream channels: field and experimental observations. Water Resour. Res. 34, 3169-3179.

Clayton, J.A., Pitlick, J., 2008. Persistence of the surface texture of a gravel-bed river during a large flood, Earth Surf. Proc. Land., 33, 661-673. doi:10.1002/esp.1567.

Curran, J., Waters, K.A., 2014. The importance of bed sediment sand content for the structure of a static armor layer in a gravel bed river, J. Geophys. Res.-Earth, 119, 1484–1497, doi:10.1002/2014JF003143.

Dudill, A., Frey, P., Church, M., 2017. Infiltration of fine sediment into a coarse mobile bed: a phenomenological study. Earth Surf. Process. Landforms, 42. 1171-1185. doi: 10.1002/esp.4080.

Ferdowsi, B., Ortiz, C.P., Houssais, M., Jerolmack., D.J., 2017. River-bed armouring as a granular segregation phenomenon. Nature Comm., 8, 1363, doi:10.1038/s41467-017-01681-3.

Frostick, L.E., Lucas, P.M., Reid, I., 1984. The infiltration of fine matrices into coarse-grained alluvial sediments and its implications for stratigraphical interpretation. J. Geol. Soc. 141, 955–965. http://dx.doi.org/10.1144/gsjgs.141.6.0955.

Guney, M.S., Bombar, G., Aksoy, A.O., 2013. Experimental Study of the Coarse Surface Development Effect on the Bimodal Bed-Load Transport under Unsteady Flow Conditions. J. Hydraul. Eng., 139(1), 12-21.

Gunsolus, E.H., Binns, A.D., 2018. Effect of morphologic and hydraulic factors on hysteresis of sediment transport rates in alluvial streams. River Res Applic. 34, 183–192.

Hassan, M.A., Egozi, R., Parker, G., 2006. Experiments on the effect of hydrograph characteristics on vertical grain sorting in gravel bed rivers, Water Resour. Res., 42, W09408. doi:10.1029/2005WR004707.

Haynes, H., Pender, G., 2007. Stress history effects on graded bed stability. J. Hydraul. Eng. 133 (4), 343–349. http://dx.doi.org/10.1061/(ASCE)0733-9429(2007)133:4(343).

Haynes, W.B., 1930. Studies in the physical properties of soil: V. The hysteresis effect in capillary properties, and the modes of moisture associated therewith. J Agric Sci. 20, 97-116.

Humphries, R., Venditti, J.G., Sklar, L.S.,Wooster, J.K., 2012. Experimental evidence for the effect of hydrographs on sediment pulse dynamics in gravel-bedded rivers. Water Resour. Res. 48, W01533. http://dx.doi.org/10.1029/2011WR010419.

Karimaee Tabarestani, M., Zarrati, A.R., 2015. Sediment transport during flood event: a review. Int. J. Environ. Sci. Technol. 12(2), 775-788.

Kuhnle, R.A., 1992. Bed load transport during rising and falling stages on two small streams. Earth Surf. Process. Landf. 17, 191–197. http://dx.doi.org/10.1002/esp.3290170206.

Langlois, J.L., Johnson, D.W., Mehuys, G.R., 2005. Suspended sediment dynamics associated with snowmelt runoff in a small mountain stream of Lake Tahoe (Nevada). Hydrol. Process. 19, 3569-3580. http://dx.doi.org/10.1002/hyp.5844.

Lee, T.L., Liu Y.L., Cheng K.H., 2004. Experimental investigation of bedload transport processes under unsteady flow conditions. Hydrol. Processes. 18(13), 2439–245. doi:10.1002/hyp.1473.

Mallakpour, I., Villarini, G., 2015. The changing nature of flooding across the central United States. Nature Climate Change, 5, 250-254. doi:10.1038/nclimate2516.

Mao, L., 2012. The effect of hydrographs on bed load transport and bed sediment spatial arrangement. J. Geophys. Res. Earth Surf. 117, F03024. http://dx.doi.org/10.1029/2012JF002428.

Mao, L., Carrillo., 2017. Temporal dynamics of suspended sediment transport in a glacierized Andean basin. Geomorphology, 287, 116-125.

Mao, L., Cooper, J.R., Frostick, L.E., 2011. Grain size and topographical differences between static and mobile armor layers. Earth Surf. Process. Landf. 36, 1321–1334. http://dx.doi.org/10.1002/esp.2156.

Mao, L., Dell'Agnese, A., Huincache, C., Penna, D., Engel, M., Niedrist, G., Comiti, F., 2014. Bedload hysteresis in a glacier-fed mountain river. Earth Surf. Process. Landf. 39(7), 964–976. http://dx.doi.org/10.1002/esp.3563.

Marion, A, Fraccarollo, L., 1997. Experimental investigation of mobile armouring development. Water Res. Res. 33(6), 1447-1453.

Marquis, G.A., Roy, A.G., 2012. Using multiple bed load measurements: toward the identification of bed dilation and contraction in gravel-bed rivers. J. Geophys. Res. 117, F01014. http://dx.doi.org/10.1029/2011JF002120.

Masteller, C.C., Finnegan N.J. 2017. Interplay between grain protrusion and sediment entrainment in an experimental flume, J. Geophys. Res. Earth Surf., 122, 274–289.

Norbiato, D., Borga, M., 2008. Analysis of hysteretic behaviour of a hillslope-storage kinematic wave model for subsurface flow. Adv. in Water Resour. 31, 118-131.

Ockelford, A., Haynes, H., 2013. The impact of stress history on bed structure. Earth Surf. Process. Landforms. 38. 717-727.

Parker, G., Toro-Escobar, C.M., 2002. Equal mobility of gravel in streams: the remains of the day. Water Res. Res. 38(11), 1264. DOI.10.1029/2001WR000669

Parker, G., Dhamotharan, S., Stefan, H., 1982. Model experiments on mobile, paved gravel bed streams. Water Res. Res. 18(5), 1395-1408.

Piedra, M.M, Haynes, H., Hoey, T.B., 2012. The spatial distribution of coarse surface grains and the stability of gravel river beds. Sedimentology 59(3), 1014-1029. Doi: 10.1111/j.1365-3091.2011.01290.x

Powell, D.M., Ockelford A., Rice S.P., Hillier J.K., Nguyen T., Reid I., Tate N.J., Ackerley D., 2016. Structural properties of mobile armors formed at different flow strengths in gravel-bed rivers. J. Geophys. Res. Earth Surf. 121, 1494-1515. doi:10.1002/2015JF003794.

Recking, A., Liebault, F., Peteuil, C., Jolimet, T., 2012. Testing bedload transport equations with consideration of time scales. Earth Surf. Process. Landf., 37, 774-789.

Reid, I., Frostick, L.E., Layman, J.T., 1985. The incidence and nature of bedload transport during flood flows in coarse-grained alluvial channels. Earth Surf. Process. Landf. 10, 33–44. http://dx.doi.org/10.1002/esp.3290100107.

Rickenmann, D., 2018. Variability of bed load transport during six summers of continuous measurements in two Austrian mounta in streams (Fischbach and Ruetz). Water Res. Res. 54, 107.131.

Salathé, E.P., Hamlet A.F., Mass C.F., Lee S., Stumbaugh M., Steed R., 2014. Estimates of Twenty-First-Century Flood Risk in the Pacific Northwest Based on Regional Climate Model Simulations. J. Hydrometeor., 15, 1881-1899.

Seitz, L., Haas, C., Noack, M., Wieprecht, S., 2018. From picture to porosity of river bed material using Structure-from-Motion with Multi-View-Stereo. Geomorphology 306, 80-89. https://doi.org/10.1016/j.geomorph.2018.01.014

Vázquez-Tarrío, D., Menéndez-Duarte, R. 2015. Bedload transport rates for coarse-bed streams in an Atlantic region (Narcea River, NW Iberian Peninsula). Geomorphology 217, 1-14. doi.org/10.1016/j.geomorph.2014.04.015.

Vericat, D., Church, M., Batalla, R.J., 2006. Bed load bias: comparison of measurements obtained using two Helley-Smith samplers (76 and 152 mm) in a gravel-bed river. Water Resour. Res. 42, W01402. http://dx.doi.org/10.1029/2005WR004025.

Wang, L., Cuthbertson, A.J.S., Pender, G., Cao, Z., 2015. Experimental investigations of graded sediment transport under unsteady flow hydrographs. Int. J. Sediment Res., 30, 306-320.

Waters, K.A., Curran, J.C., 2015. Linking bed morphology changes of two sediment mixtures to sediment transport predictions in unsteady flows. Water Resour. Res., 51, 2724-2741. doi:10.1002/2014WR016083

Wilcock, P.R., 2001. The flow, the bed, and the transport: interaction in flume and field. In Gravel-bed Rivers V, Mosley M (ed.). NZ Hydrological Society: Wellington; 183–219.

Wilcock, P.R., Crowe, J.C., 2003. Surface-based transport model for mixed-size sediment. J. Hydraul. Eng. 129 (2), 120–128. http://dx.doi.org/10.1061/(ASCE)0733-9429(2003)129:2(120).

Wilcock, P.R., DeTemple B.T., 2005. Persistence of armor layers in gravel-bed streams. Geophys. Res. Lett. 32, L08402. doi:10.1029/2004GL021772.

Woodget, A.S., Fyffe, C., Carbonneau, P.E., 2018. From manned to unmanned aircraft: Adapting airborne particle size mapping methodologies to the characteristics of sUAS and SfM. Earth Surf. Process. Landf. 43(4), 857-870. https://doi.org/10.1002/esp.4285

Zuecco, G., Penna, D., Borga, M., van Meerveld, H.J., 2016. A versatile index to characterize hysteresis between hydrological variables at the runoff event timescale. Hydrol. Processes. 30(9), 1449-1466.

Figure Caption

Fig. 1. Sediment transport rates (q_s), grain size of the bed surface (D_{50} and D_{84}), and grain size of transported sediments (D_{50} and D_{84}) during experiments simulating sequences of the same hydrographs (HHH, MMM, and LLL).

Fig. 2. The average transport rate (q_s, on the left), grain size of transported sediment ($D_{50transp}$ and $D_{84transp}$, in the middle), and grain size of surface sediment (D_{50surf} and D_{84surf}, on the right) at flow steps of sequences of the same hydrographs (HHH, MMM, and LLL). Rising limbs of hydrographs are identified by lines with markers (and R notation) and falling limbs by dashed lines (and F notation). Solid squares represent the sediment transport rates at long-term equilibrium conditions during sediment recirculation experiments (from Mao et al., 2011).

Fig. 2. Sediment transport rates (q_s), grain size of the bed surface (D_{50} and D_{84}), and grain size of transported sediments (D_{50} and D_{84}) during experiments simulating sequences of the different hydrographs (LMH, HML, HLH, and LHL).

Fig. 4. The average transport rate (q_s, on the left), grain size of transported sediment ($D_{50transp}$ and $D_{84transp}$, in the middle), and grain size of surface sediment (D_{50surf} and D_{84surf}, on the right) at flow steps of sequences of the different hydrographs (LMH, HML, HLH, and LHL). Rising limbs of hydrographs are identified by lines with markers (and R notation) and falling limbs by dashed lines (and F notation). Solid squares represent the sediment transport rates at long-term equilibrium conditions during sediment recirculation experiments (from Mao et al., 2011).

Fig. 5. The average transport rate (q_s) at the peak flow for all simulated flood sequences.

Fig. 6. Hysteretic index H calculated based on the flow discharge (q) and the average transport rate (q_s). The pattern is clockwise for $H > 1$ and counterclockwise for $H < 1$.

Fig. 7. Hysteretic index H calculated based on the flow discharge (q) and the size of transported sediments ($D_{84transp}$). The pattern is clockwise for $H > 1$ and counterclockwise for $H < 1$.

Fig. 8. Percentage difference in the sediment transport rate of an event compared to that of a previous event of the same magnitude.

TABLES

Table 1

Unit discharge (in m^2 s^{-1}) and duration (in minutes) of the flow steps composing the sequences of three hydrographs (H indicates the short-duration/high-magnitude, L the long-duration/low-magnitude event, and M the intermediate event).

		HHH		MMM		LLL		LMH		HML		HLH		LHL	
	Step	q (m^2 s^{-1})	Dur (min)	q (m^2 s^{-1})	Dur (min)	q (m^2 s^{-1})	Dur (min)	q (m^2 s^{-1})	Dur (min)	q (m^2 s^{-1})	Dur (min)	q (m^2 s^{-1})	Dur (min)	q (m^2 s^{-1})	Dur (min)
Hydrograph a	Rising	0.044	15	0.038	60	0.024	120	0.024	120	0.044	15	0.044	15	0.024	120
	Rising	0.054	15	0.044	60	0.031	120	0.031	120	0.054	15	0.054	15	0.031	120
	Rising	0.064	15	0.049	60	0.038	120	0.038	120	0.064	15	0.064	15	0.038	120
	Peak	0.085	15	0.054	60	0.044	120	0.044	120	0.085	15	0.085	15	0.044	120
	Falling	0.064	15	0.049	60	0.038	120	0.038	120	0.064	15	0.064	15	0.038	120
	Falling	0.054	15	0.044	60	0.031	120	0.031	120	0.054	15	0.054	15	0.031	120
	Falling	0.044	15	0.038	60	0.024	120	0.024	120	0.044	15	0.044	15	0.024	120
Hydrograph b	Rising	0.044	15	0.038	60	0.024	120	0.038	60	0.038	60	0.024	120	0.044	15
	Rising	0.054	15	0.044	60	0.031	120	0.044	60	0.044	60	0.031	120	0.054	15
	Rising	0.064	15	0.049	60	0.038	120	0.049	60	0.049	60	0.038	120	0.064	15
	Peak	0.085	15	0.054	60	0.044	120	0.054	60	0.054	60	0.044	120	0.085	15
	Falling	0.064	15	0.049	60	0.038	120	0.049	60	0.049	60	0.038	120	0.064	15
	Falling	0.054	15	0.044	60	0.031	120	0.044	60	0.044	60	0.031	120	0.054	15
	Falling	0.044	15	0.038	60	0.024	120	0.038	60	0.038	60	0.024	120	0.044	15
Hydrograph c	Rising	0.044	15	0.038	60	0.024	120	0.044	15	0.024	120	0.044	15	0.024	120
	Rising	0.054	15	0.044	60	0.031	120	0.054	15	0.031	120	0.054	15	0.031	120
	Rising	0.064	15	0.049	60	0.038	120	0.064	15	0.038	120	0.064	15	0.038	120
	Peak	0.085	15	0.054	60	0.044	120	0.085	15	0.044	120	0.085	15	0.044	120
	Falling	0.064	15	0.049	60	0.038	120	0.064	15	0.038	120	0.064	15	0.038	120
	Falling	0.054	15	0.044	60	0.031	120	0.054	15	0.031	120	0.054	15	0.031	120
	Falling	0.044	15	0.038	60	0.024	120	0.044	15	0.024	120	0.044	15	0.024	120

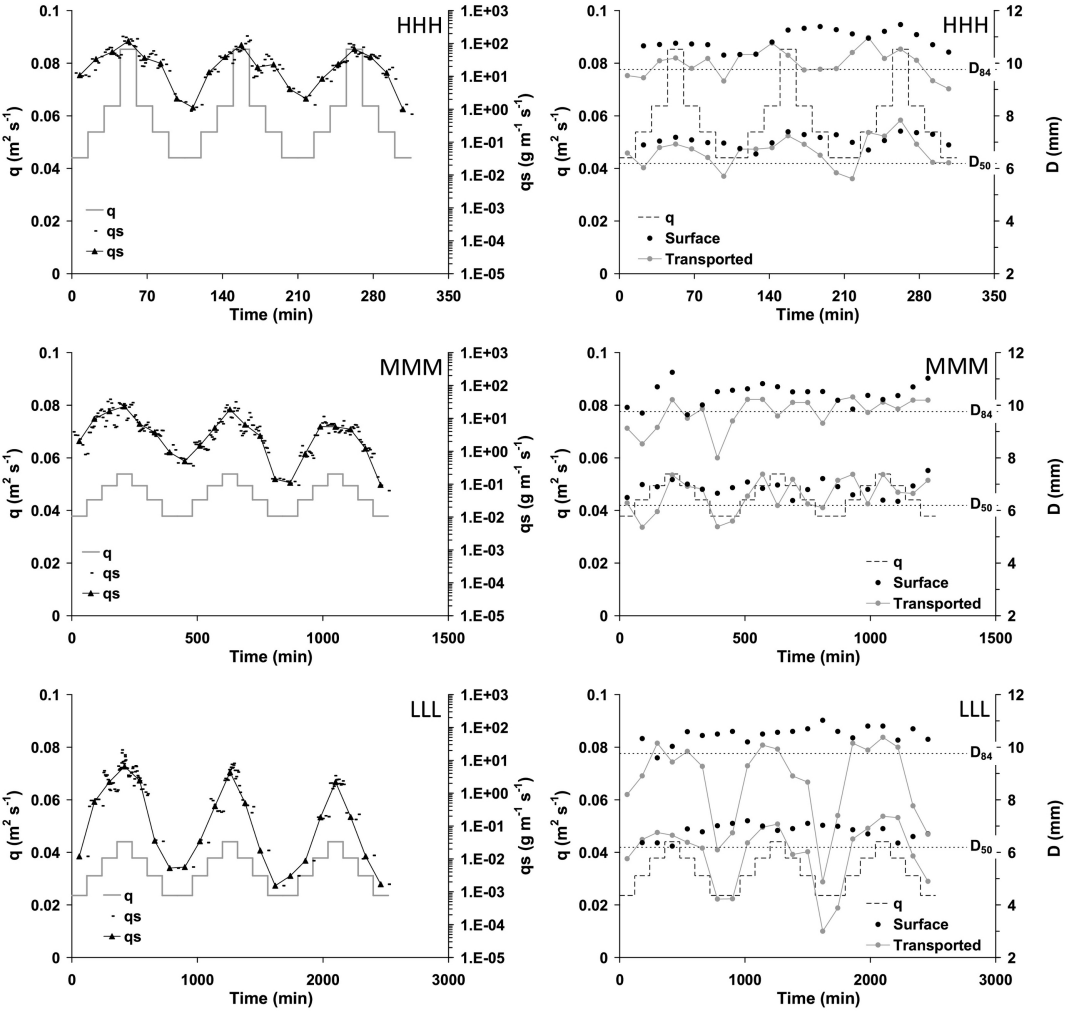
HHH
MMM
LLL
q (m² s⁻¹)
qs (g m⁻¹ s⁻¹)
D (mm)
Time (min)
q
qs
qs
Surface
Transported
D84
D50

Figure 1

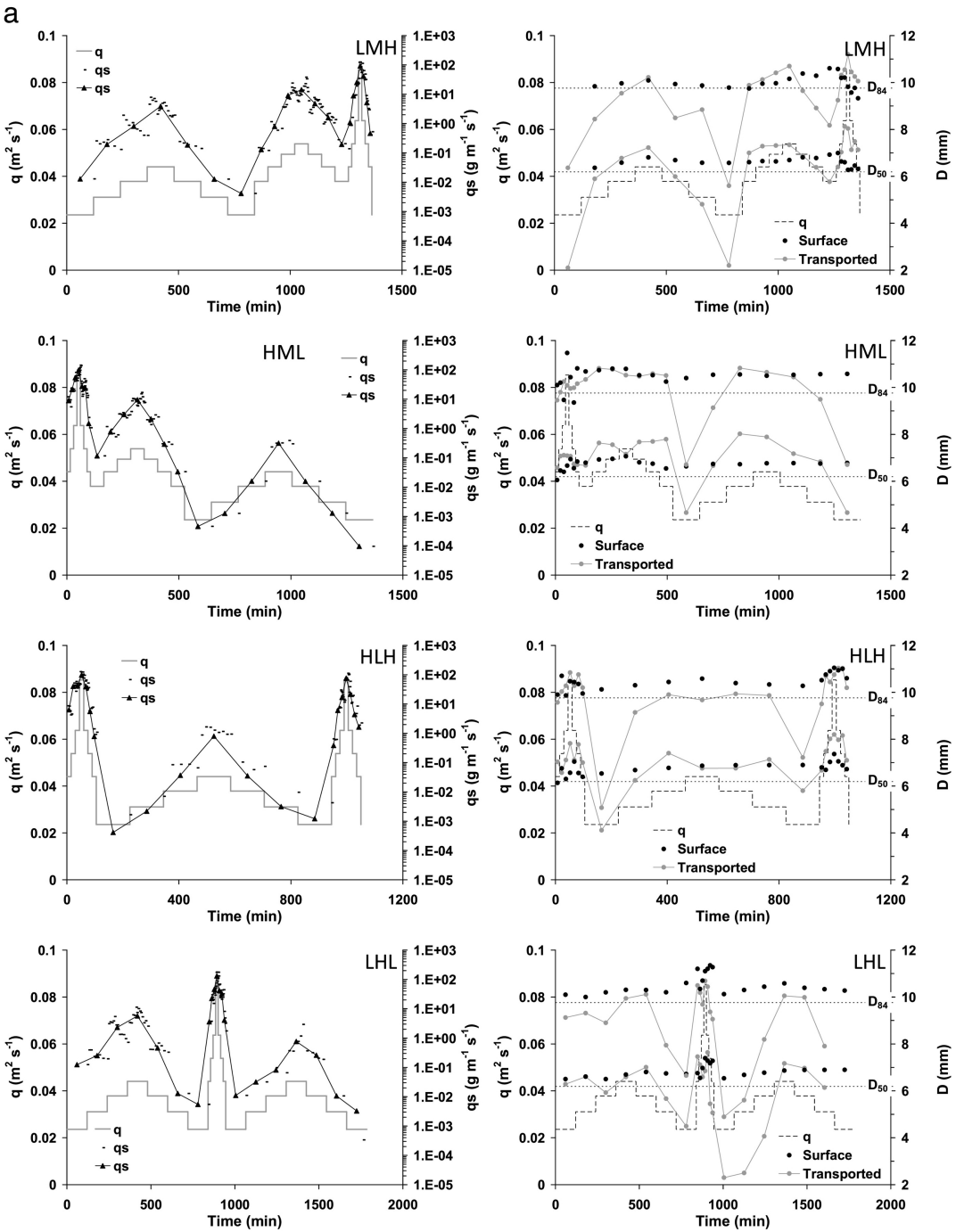
a
LMH
HML
HLH
LHL
q
qs
qs
Surface
Transported
D_{84}
D_{50}
Time (min)
q (m^2 s^{-1})
qs (g m^{-1} s^{-1})
D (mm)

Figure 2a

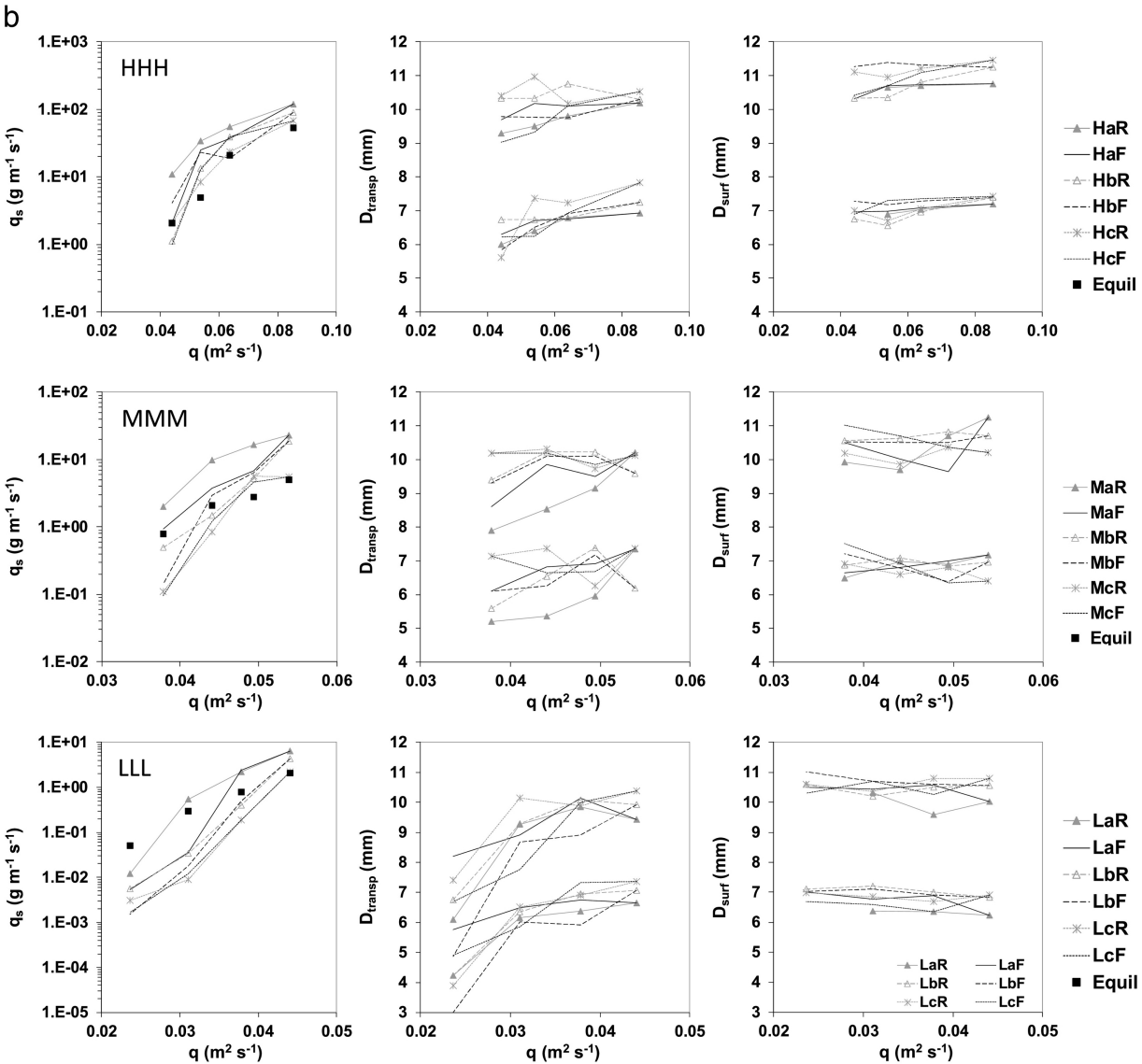
b
HHH
MMM
LLL
q_s (g m^{-1} s^{-1})
D_{transp} (mm)
D_{surf} (mm)
q (m^2 s^{-1})
HaR
HaF
HbR
HbF
HcR
HcF
Equil
MaR
MaF
MbR
MbF
McR
McF
LaR
LaF
LbR
LbF
LcR
LcF

Figure 2b

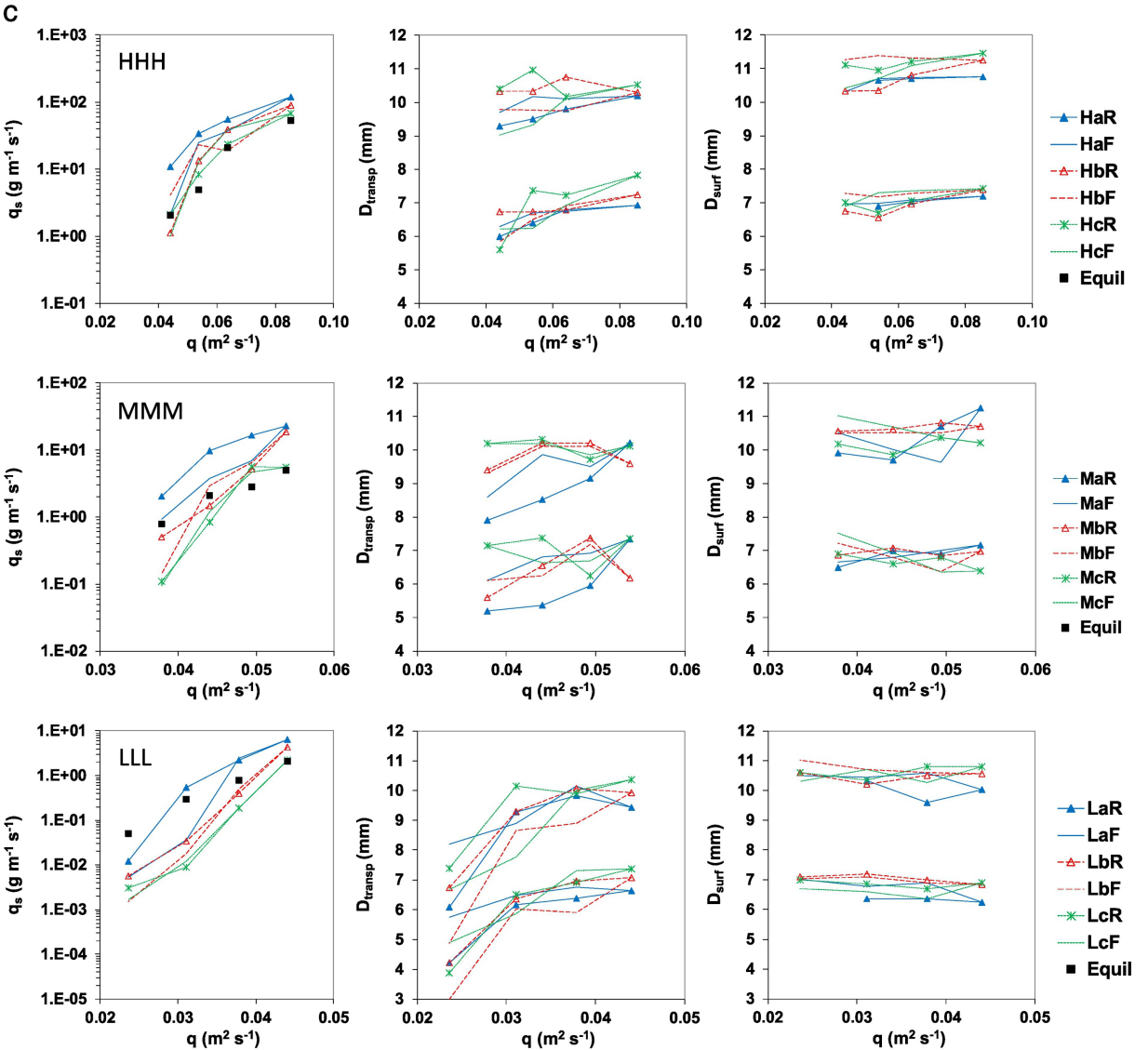
C
HHH
MMM
LLL
q_s (g m^{-1} s^{-1})
D_{transp} (mm)
D_{surf} (mm)
q (m^2 s^{-1})
HaR
HaF
HbR
HbF
HcR
HcF
Equil
MaR
MaF
MbR
MbF
McR
McF
LaR
LaF
LbR
LbF
LcR
LcF

Figure 2c

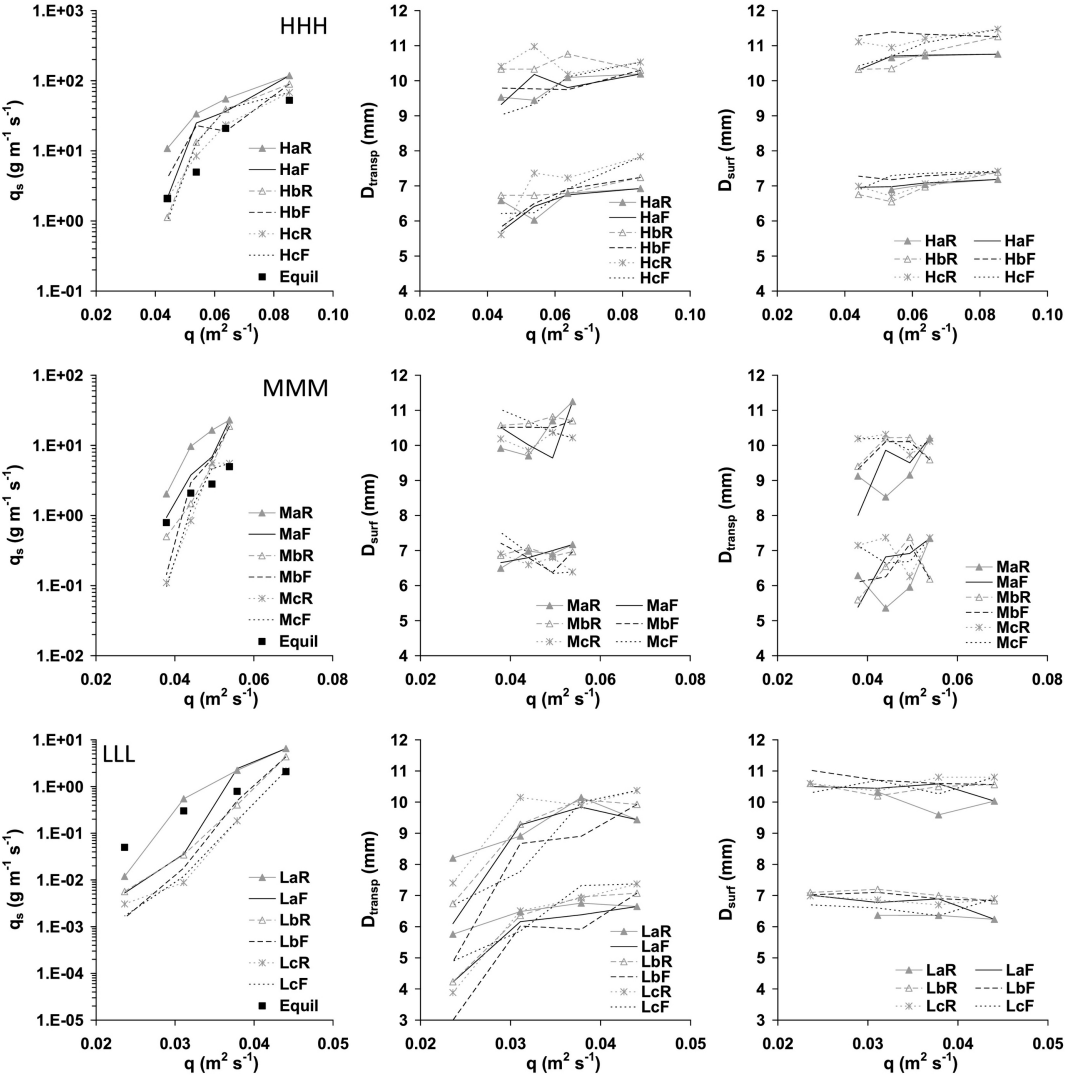
HHH
MMM
LLL
q_s (g m^{-1} s^{-1})
D_{transp} (mm)
D_{surf} (mm)
q (m^2 s^{-1})
HaR
HaF
HbR
HbF
HcR
HcF
Equil
MaR
MaF
MbR
MbF
McR
McF
LaR
LaF
LbR
LbF
LcR
LcF

Figure 3

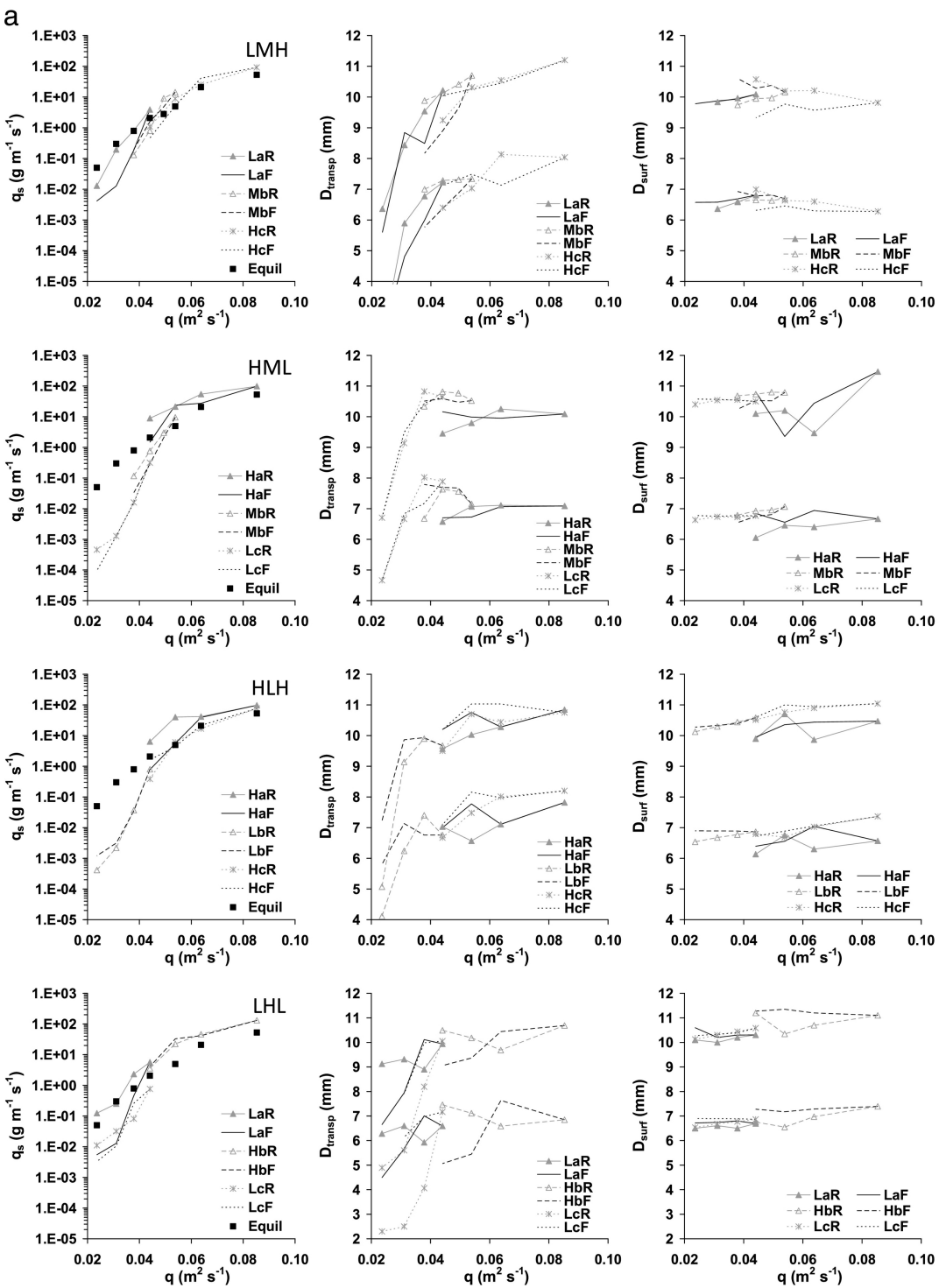
a
LMH
HML
HLH
LHL
q_s (g m^{-1} s^{-1})
D_{transp} (mm)
D_{surf} (mm)
q (m^2 s^{-1})
LaR
LaF
MbR
MbF
HcR
HcF
Equil
HaR
HaF
LcR
LcF
HbR
HbF
LbR
LbF

Figure 4a

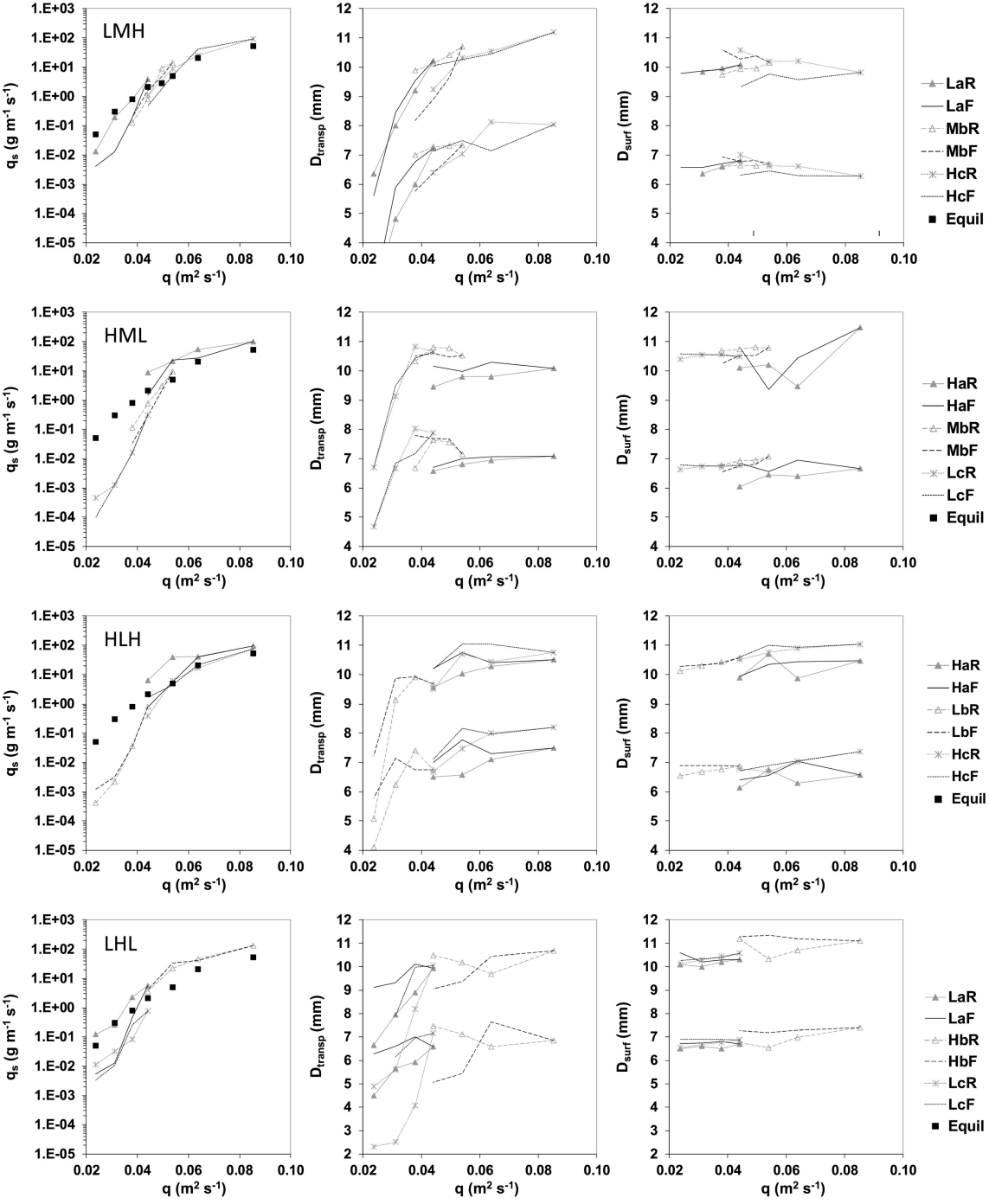
LMH
HML
HLH
LHL
q_s (g m^{-1} s^{-1})
D_{transp} (mm)
D_{surf} (mm)
q (m^2 s^{-1})
LaR
LaF
MbR
MbF
HcR
HcF
Equil
HaR
HaF
LcR
LcF
LbR
LbF
HbR
HbF

Figure 4b

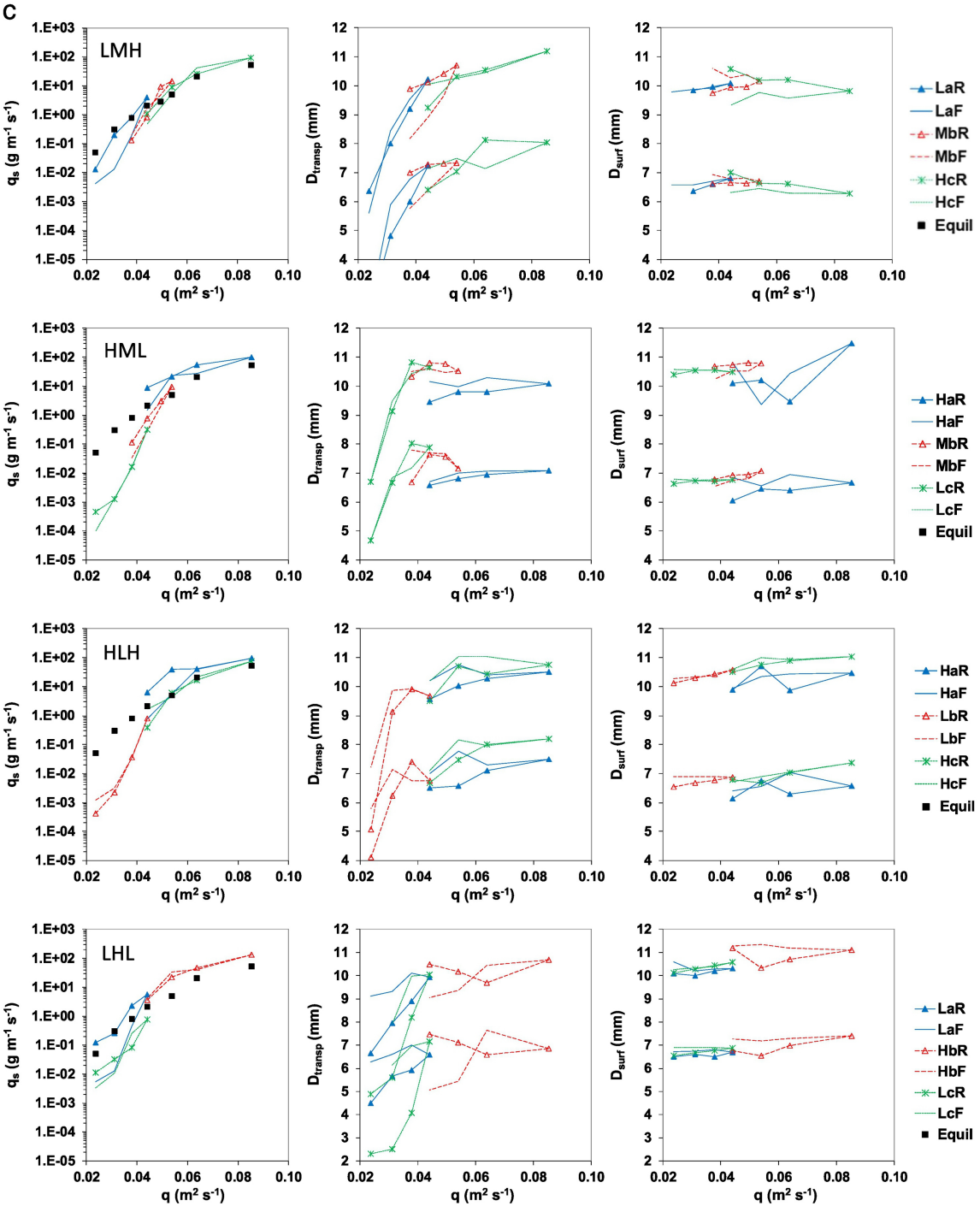
C
LMH
HML
HLH
LHL
q_s (g m^{-1} s^{-1})
D_{transp} (mm)
D_{surf} (mm)
q (m^2 s^{-1})
LaR
LaF
MbR
MbF
HcR
HcF
Equil
HaR
HaF
MbR
MbF
LcR
LcF
Equil
HaR
HaF
LbR
LbF
HcR
HcF
Equil
LaR
LaF
HbR
HbF
LcR
LcF
Equil

Figure 4c

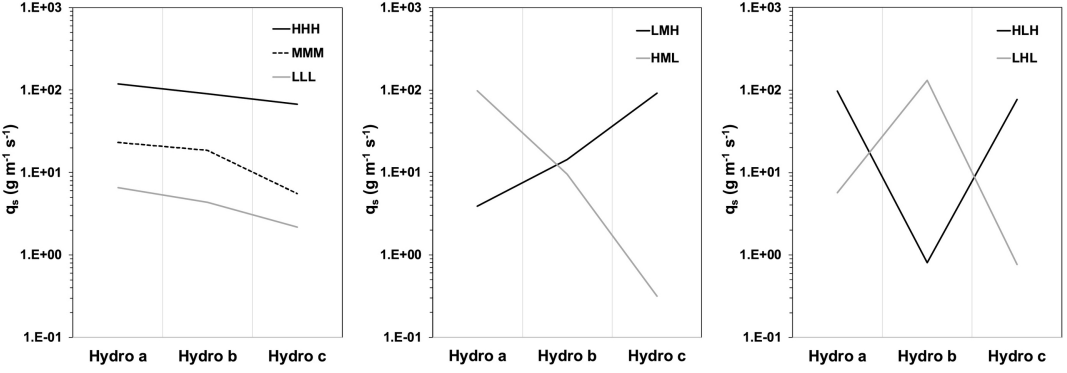
1.E+03
1.E+02
1.E+01
1.E+00
1.E-01
q_s (g m^{-1} s^{-1})
HHH
MMM
LLL
LMH
HML
HLH
LHL
Hydro a
Hydro b
Hydro c

Figure 5

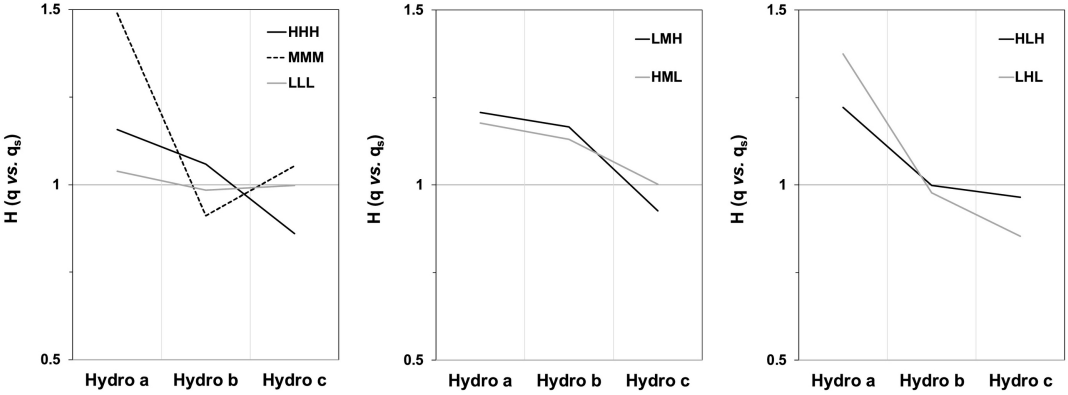
1.5
1
0.5
H (q vs. q_s)
HHH
MMM
LLL
Hydro a
Hydro b
Hydro c
LMH
HML
HLH
LHL

Figure 6

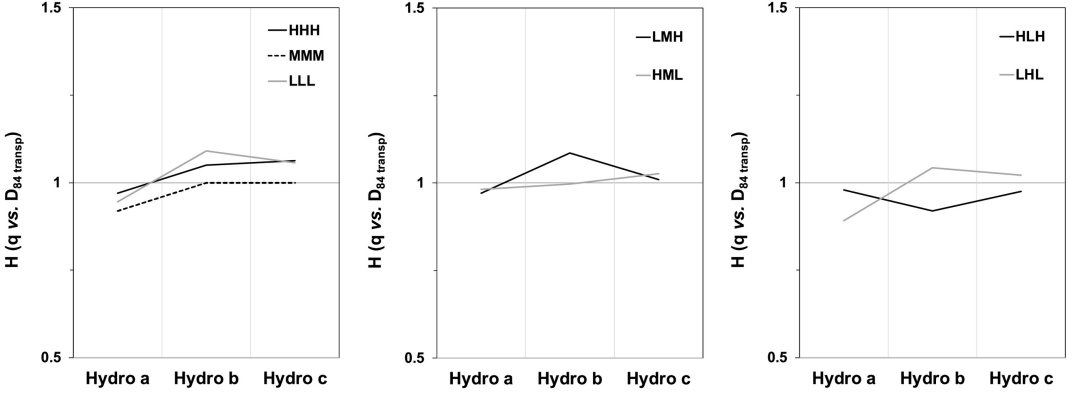
1.5
1
0.5
H (q vs. D84 transp.)
HHH
MMM
LLL
Hydro a
Hydro b
Hydro c
LMH
HML
HLH
LHL

Figure 7

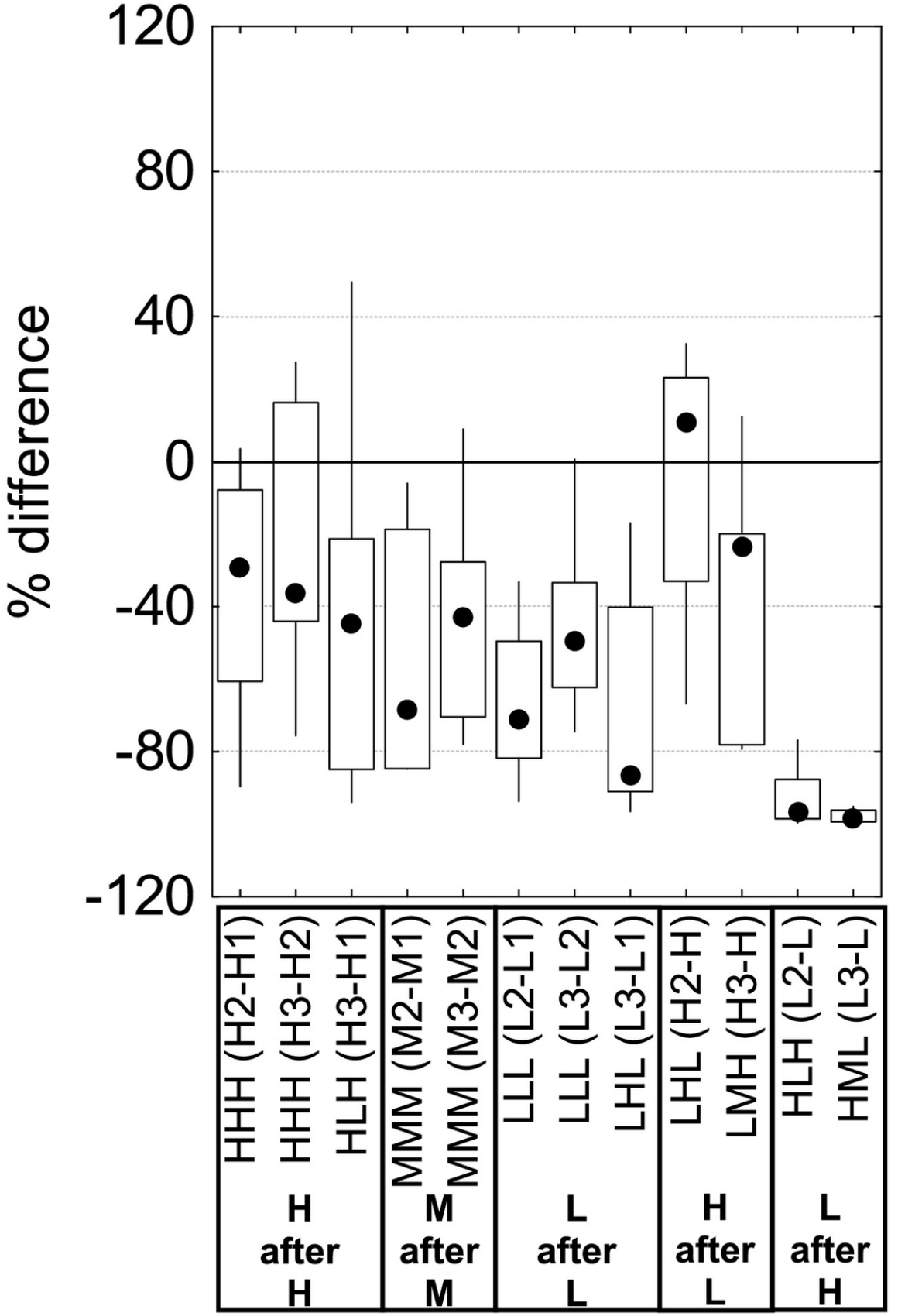
120
80
40
0
-40
-80
-120
% difference
HHH (H2-H1)
HHH (H3-H2)
HLH (H3-H1)
MMM (M2-M1)
MMM (M3-M2)
LLL (L2-L1)
LLL (L3-L2)
LHL (L3-L1)
LHL (H2-H)
LMH (H3-H)
HLH (L2-L)
HML (L3-L)
H after H
M after M
L after L
H after L
L after H

Figure 8